(Received 20 October 2023, Accepted 28 November 2023, Scheduled 4 December 2023)

A Research Based on Transmissive Amplitude-Phase Dual Control about Generating High Quality Vertex Beam

Honggang Hao, Pan Tang*, Bao Li, and Zhonglyu Cai

School of Optoelectronic Engineering, Chongqing University of Posts and Telecommunications, Chongqing 400065, China

ABSTRACT: Orbital angular moment modes (OAMs) have been proven to be promising resources for increasing communication capacity. To generate wideband and high purity OAM, we have proposed a transmitting metasurface with amplitude-phase dual control. The proposed unit cell is a novel split ring structure with upper and lower grating-like structures. By changing the direction angle and rotation angle of the split-ring unit, the cross-polarization phase response and amplitude response of the unit are controlled respectively. The amplitude distribution of the metasurface array is calculated using Chebyshev synthesis method (CSM). We designed metasurface arrays with mode numbers $l = 1, 2, 3$, and it generated high purity OAM beams in the frequency band of 22–32 GHz. Compared with traditional phase-control metasurface, amplitude-phase control surface can effectively improve the quality of OAM generation. The results have verified the accuracy of the proposed method, and the proposed method has potential applications in future communication system.

1. INTRODUCTION

With the development of wireless communication technology and the increasing number of mobile terminals, frequency and polarization reuse technologies are becoming increasingly difficult to meet the demands of information communication. However, the OAM carried by vortex electromagnetic waves [1] has spiral phase distribution, circular amplitude distribution, and orthogonality between modes, due to its theoretically infinite number of orthogonal mode numbers, that can greatly improve spectrum utilization and significantly improve communication speed and information capacity of communication systems [2, 3]. The research on OAM has attracted widespread attention from researchers. Currently, there are several methods for generating OAM beams, including spiral phase plates [4], antenna arrays [5], and metasurfaces [6]. Nevertheless, OAM beams are generated using spiral phase plates with a single mode and limited processing accuracy. Antennas-generated OAM modes are more flexible while they require complex feeding networks, which increase as the size of the structure expands. Metasurface, as a planar structure, is easy to manufacture and generate high-gain beams with small divergence angles, which makes them popular among researchers [7–9].

Metasurface is sub-wavelength two-dimensional artificial electromagnetic materials. It is the two-dimensional form of electromagnetic metamaterials. By arranging metasurface in periodic or non-periodic arrays, effective control of the amplitude, phase, or polarization characteristics of electromagnetic waves can be achieved. It also has characteristics not found in natural materials, such as zero and negative refractive indices. Utilizing these characteristics, functions such as beam deflection, beam shaping, and OAM beam generation can be achieved [10–13]. In recent years, there have been many reports on the use of metasurfaces to generate OAM beams. In [14], Arkram et al. proposed a photon spin-based transmissive metasurface that generates OAM beams using the Pancharatnam-Berry (PB) phase mechanism. In [15], Ji et al. designed a dual-frequency vortex beam surface capable of generating different OAM modes. It used resonant geometric unit structures to generate phase distributions, and used linear and circular polarizations to generate $l = 1$ and $l = 2$ OAM beams, respectively. In [16], a broadband transmissive surface with a combination of double-ring structures was proposed to generate 1st order OAM beams using circular arrays. However, the mentioned metasurface only generates vortex waves based on phase distributions. The amplitude distribution within the metasurface plays a crucial role in controlling the energy distribution of electromagnetic wave beams. In [17, 18], amplitude and phase modulation are utilized to achieve beam energy control and sidelobe suppression. Based on antenna theory, the Chebyshev synthesis method (CSM) can effectively reduce sidelobes in electromagnetic wave beam transmission and improve beam directionality [19, 20]. Though some scholars have used amplitude and phase simultaneously to generate OAM beams [21], there are still few research reports in this area. In vortex beam systems, issues such as mode crosstalk, large divergence, and narrow bandwidth still need further research. OAM purity is an important indicator of OAM beam quality. Generating high-purity vortex beams can not only effectively suppress mode crosstalk but also help receivers in detect and identify vortex beams. Wideband OAM beam generation is crucial for the practical application of OAM technology in communication systems [16, 22, 23]. Therefore, using amplitude and phase modulation to improve the generation purity of OAM beams has certain research significance.

* Corresponding author: Pan Tang (s210401025@stu.cqupt.edu.cn).

In this work, we propose a transmissive amplitude-phase control metasurface and combine the surface with antenna theory CSM for generating OAM beams. The designed surface generates OAM beams by phase control while the amplitude distribution of the metasurface is calculated using CSM of antenna theory to improve the quality of OAM beams. Through theoretical analysis, we calculated the transmission response of the proposed amplitude-phase control unit to obtain its performance in modulating amplitude response. Through simulation, we achieved simultaneous modulation of transmission amplitude and phase response within a wide bandwidth. Simulation results demonstrated that this unit exhibited high flexibility in modulating cross-polarization transmission amplitude and phase within a wide bandwidth, achieving full coverage of both amplitude and phase. Subsequently, from an application perspective, we analysed the design and fabrication of a high-quality OAM beam-generating metasurface and mode purity. Full-wave simulation results confirmed the feasibility and effectiveness of our design method.

2. DESIGN OF METASURFACE ELEMENT

In the design of metasurfaces, the highly symmetrical structure is required to ensure effective modulation of electromagnetic waves. Simultaneously, a better amplitude modulation effect necessitates precise control over the polarization conversion transmission rate of electromagnetic waves by the unit.

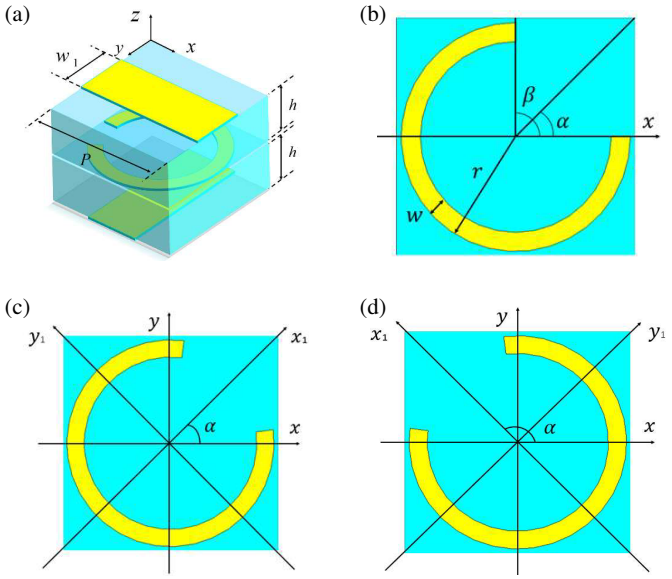

FIGURE 1. The schematic of the proposed metasurface unit structure: (a) shows the overall structure, (b), (c), and (d) depict the split-ring structure under different α and β angles.

Therefore, the metasurface unit is designed as follows. The proposed transmitting array unit cell with geometry layout is illustrated in Figure 1(a) and Figure 1(b). There are two dielectric layers and three identical metallic layers. The two rectangular metal patches in the upper and lower layers are perpendicular to each other. The arrangement of the three layers of metasurfaces forms a Fabry-Pérot-like cavity, enabling multiple reflections and polarization conversions within the cavity and therefore significantly enhancing the overall polarization conversion efficiency. By appropriately adjusting the resonator geometric parameters, the overall co-polarized reflection can be minimized due to the destructive interference of the multiple reflections [7]. During the process, the periodicity of the unit cell is $P = 2.5\,\text{mm}$. The substrate F4B is used with material specification $\varepsilon = 2.65$, and the dielectric loss constant is $\tan\delta = 0.001$. The thickness of the substrate is $h = 1\,\text{mm}$. The width of the metal patches is $w_1 = 1\,\text{mm}$, and the length is equal to the unit period P. The metal patch in the middle layer is an open circular metal ring with a split angle and direction angle distribution denoted by α and β, respectively. The outer radius of the metal ring is $r = 1.2\,\text{mm}$, while its thickness is $w = 0.2\,\text{mm}$. To achieve full coverage of the amplitude-phase transmission response for the unit, the thickness h of the dielectric layer should be less than or equal to $h = 1\,\text{mm}$. Keeping other parameters constant, the transmission amplitude and phase values of the designed unit are obtained by regulating the direction angle α and split angle β. The following theoretical analysis is used to calculate the modulation effect of the designed unit. The modulation effect of the designed unit is calculated by theoretical analysis using Equations (1) and (2) shown in Figure 1(c) and Figure 1(d), respectively.

$$\hat{e}_{x_1} = \hat{e}_x \cos\alpha + \hat{e}_y \sin\alpha \tag{1}$$

$$\hat{e}_{y_1} = -\hat{e}_x \sin\alpha + \hat{e}_y \cos\alpha \tag{2}$$

When a y-polarized electromagnetic wave is vertically incident on the unit cell shown in Figure 1(c), it can be decomposed into orthogonal components. The vector electric field values after the electromagnetic wave enters the unit cell are given by Equation (3), and the transmitted response generated by the electromagnetic wave after transmission through the unit cell is expressed as the vector value shown in Equation (4):

$$\vec{E}_{i1} = E_0\hat{e}_y = E_0\left(\hat{e}_{x_1}\sin\alpha + \hat{e}_{y_1}\cos\alpha\right) \tag{3}$$

$$\vec{E}_{t_1} = E_0\left(T_{x_1}\sin x\hat{e}_{x_1} + T_{y_1}\cos\alpha\hat{e}_{y_1}\right) \tag{4}$$

where T_{x1} and T_{y1} represent the transmission coefficients in the x_1 and y_1 directions, respectively. Due to the high rotational symmetry of the designed split-ring structure in space, the transmission coefficients of the structures shown in Figures 1(c) and (d) are equal. By transforming the coordinate values back into the original coordinate system, the final transmission amplitude of the unit cell can be obtained. By substituting Equations (1) and (2) into Equation (4), the vector electric field values can be expressed as shown in Equation (5).

$$\vec{E}_{t_1} = E_0\left[\frac{1}{2}\left(\left(T_{x_1} - T_{y_1}\right)\sin 2\alpha\hat{e}_x + \left(T_{x_1}\sin^2\alpha + T_{y_1}\cos^2\alpha\right)\hat{e}_y\right)\right] \tag{5}$$

Similarly, in the unit shown in Figure 1(d), the corresponding coordinate transformation equations are shown in Equations (6) and (7).

$$\hat{e}_{x_1} = -\hat{e}_x \sin\alpha + \hat{e}_y \cos\alpha \tag{6}$$

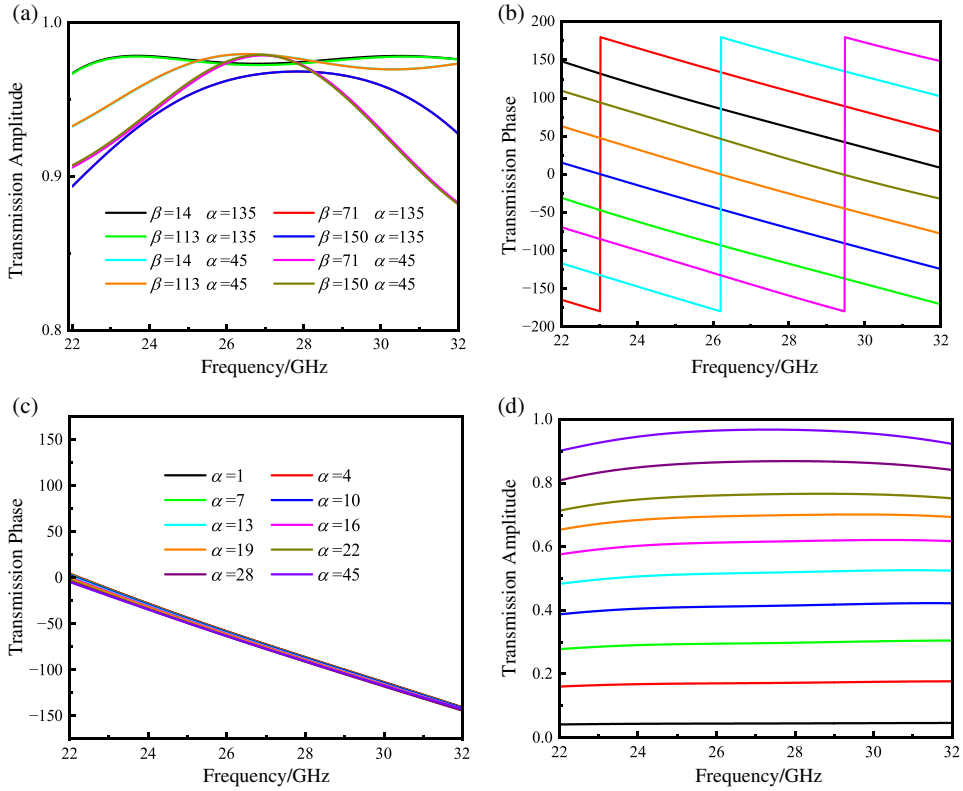

FIGURE 2. Unit transmission response at 22–32 GHz: (a) and (b) depict the variation in amplitude and phase response with β at α of 45° and 135°; (c) and (d) illustrate the distribution of phase and amplitude responses with a change in α while keeping β constant.

$$\hat{e}_{y_1} = -\hat{e}_x \cos\alpha - \hat{e}_y \sin\alpha \tag{7}$$

Correspondingly, the incident and transmitted waves for the unit shown in Figure 1(d) should be:

$$\vec{E}_{i2} = E_0\hat{e}_y = E_0\left(\hat{e}_{x_1}\cos\alpha - \hat{e}_{y_1}\sin\alpha\right) \tag{8}$$

$$\vec{E}_{t_2} = E_0\left(T_{x_1}\cos x\hat{e}_{x_1} - T_{y_1}\sin\alpha\hat{e}_{y_1}\right) \tag{9}$$

Substituting Equations (6) and (7) into Equation (9), we obtain:

$$\vec{E}_{t_2} = E_0\left[\frac{1}{2}e^{j\pi}\left(\left(T_{x_1} - T_{y_1}\right)\sin 2\alpha\hat{e}_x + \left(T_{x_1}\cos^2\alpha + T_{y_1}\sin^2\alpha\right)\hat{e}_y\right)\right] \tag{10}$$

Equations (5) and (10) indicate the transmitted vector electric field values corresponding to the unit cells in Figures 1(c) and (d). These equations show that the x-polarized transmitted waves in both cells have equal amplitudes, which are proportional to $\sin(2\alpha)$. The above analysis demonstrates that the designed split-ring unit can achieve control over the amplitude of cross-polarized waves by adjusting the direction angle α. Additionally, Equations (1), (2), (6), and (7) show that the phase difference of cross-polarized waves can be altered. In Equations (5) and (10), the x-polarized waves have a phase difference of π. This means that when the direction angle α of the unit cell is increased by 90°, the transmission phase response of cross-polarized waves can be extended.

To validate the theoretical analysis of the designed unit cell's transmission response, Commercial Software Technology, CST Microwave Studio was used for simulation analysis. The unit cell was simulated using periodic boundary conditions and Floquent ports. Figure 2 depicts the amplitude and phase responses of cross-polarized transmission of the unit cell when a y-polarized electromagnetic wave is vertically incident on the surface in the frequency range of 22 GHz to 32 GHz. As shown in Figures 2(a) and (b), when the direction angle α remains constant, varying β can change the transmission phase response of the unit cell, while the transmission amplitude remains nearly unaffected. Furthermore, Figures 2(a) and (b) demonstrate that when β takes the same value, increasing the α by $\pi/2$ results in unchanged transmission amplitude with an increase of π in the transmission phase. Figures 2(c) and (d) indicate that when β remains constant, the transmission amplitude of the unit cell increases with an increase in α. The highest transmission amplitude occurs when α is 45°. However, the variation in the direction angle has little effect on the transmission phase of the unit cell. The simulation results confirm the consistency between the designed unit cell and the theoretical analysis, validating the modulation performance of both amplitude and phase responses. The wideband characteristics of the unit in the 22 GHz to 32 GHz range make it suitable for array design in broadband metasurfaces.

3. DESIGN OF METASURFACE ARRAY

The simulation results of the unit cell in the previous section indicate that the proposed structure can achieve phase 0 to 2π

and magnitude from 0 to 1 full coverage. Metasurface with independent and controllable amplitude and phase can achieve precise control of the incident electromagnetic waves. In order to better control the generation of OAM beams, a 3-bit encoding scheme is employed to discretize the phase distribution of the proposed structure. Due to the magnitude full coverage of the structure, discretization of the magnitude distribution is not necessary. Therefore, six kinds of metasurfaces are designed to generate OAM beams in a wideband. Three of designed metasurfaces are only phase control metasurfaces (PMSs) and the other three are amplitude and phase control metasurfaces (APMSs). The mode of the generated OAM beams is $l = 1$, 2 and 3, respectively. Performance of the designed metasurfaces is compared and analyzed based on two different control strategies. On the process of generating OAM, the distribution of amplitude and phase response play crucial roles in generating high purity OAM. And the uniformity of amplitude and phase distribution is proportional to the quality of the generated OAM beams. The current distribution in metasurface affects the final amplitude response.

To make current in metasurface distribution more uniform and the generated OAM beams more focused, the amplitude distribution of the metasurface is arranged using the Chebyshev synthesis method in antenna theory, based on traditional phase control metasurface.

The required phase distribution for generating vortex beams with OAM mode l is:

$$\varphi_{\text{OAM}}(x, y) = l \cdot \arctan\left(\frac{y}{x}\right) \tag{11}$$

where (x, y) are the position coordinates of the metasurface unit, and l is the OAM mode. Using a horn antenna as the feed source requires phase compensation for the designed metasurface. The phase compensation correcting the phase distribution of the spherical wave can be expressed as:

$$\varphi_{\text{horn}}(x, y) = k_0\left((x_0 - x)^2 + (y_0 - y)^2 + z_0^2\right) \tag{12}$$

$$\varphi_m(x, y) = \varphi_{\text{horn}}(x, y) + \varphi_{\text{OAM}} \tag{13}$$

where (x_0, y_0, z_0) are the three-dimensional coordinates of the phase center of the horn. A horn antenna operating in the Ku band is used as the feed source, and the horn antenna is vertically incident on the metasurface.

When the mode of OAM is 1, 2, or 3, the corresponding final-phase distribution of the metasurface is shown in Figure 3(a). For metasurfaces that only control phase, the transmission amplitude of each unit on the metasurface is equal to 1. However, for the amplitude and phase modulation metasurface, a different design method is required for calculating the amplitude distribution.

Observing Figures 4(b), (d), and (f), it can be seen that OAM beams generated by phase-controlled metasurfaces have strong sidelobes and weak main lobe energy. Therefore, the amplitude distribution of the amplitude-phase-controlled metasurface is designed from the perspective of enhancing the energy of the main lobe beam and suppressing sidelobes. CSM is commonly used in linear array antenna design to effectively reduce sidelobe levels (SLLs) in antenna direction patterns. The first two terms of Chebyshev polynomials are $T(x) = 1$ and $T_1(x) = x$. The expression for the Nth term can be obtained using the recursive formula. The expression for the recursive formula is as follows:

$$T_n(x) = 2xT_{n-1}(x) - T_{n-2}(x) \tag{14}$$

The Chebyshev distribution obtained in [19] is one-dimensional. Here, two-dimensional Chebyshev amplitude distribution is used to arrange metasurface units. The Chebyshev vector can be directly converted into a matrix. The calculation formula is as follows:

$$A_{2D} = A'_{1D} \times A_{1D} \tag{15}$$

To reduce the number of arrays, four units are combined into one meta unit, and the surface consists of 30×30 units. The final area of the array is $150\,\text{mm}^2 \times 150\,\text{mm}^2$ ($15\lambda \times 15\lambda$). Setting the sidelobe level to -40 dB, Equation (15) is used to calculate the amplitude distribution of the surface, while this equation is calculated under plane wave incidence. Considering that the amplitude of the horn antenna is not uniform, it needs to be corrected. Equation (16) shows the corrected amplitude

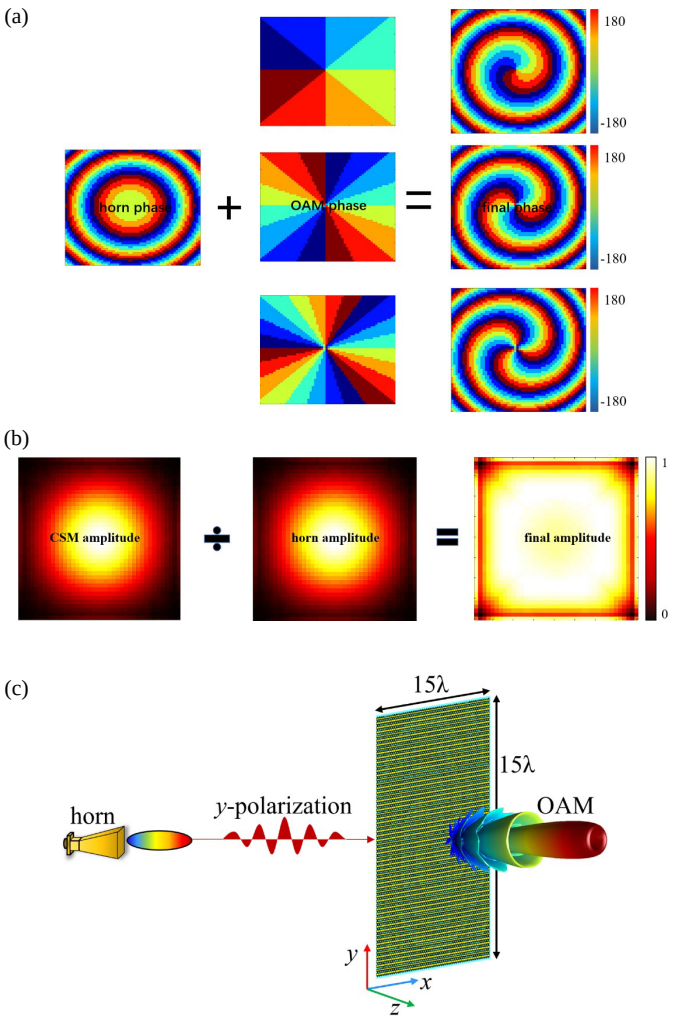

FIGURE 3. The compensation of the amplitude and phase: (a) is the phase compensation, (b) is the amplitude compensation, (c) is block diagram of the overall design metasurface.

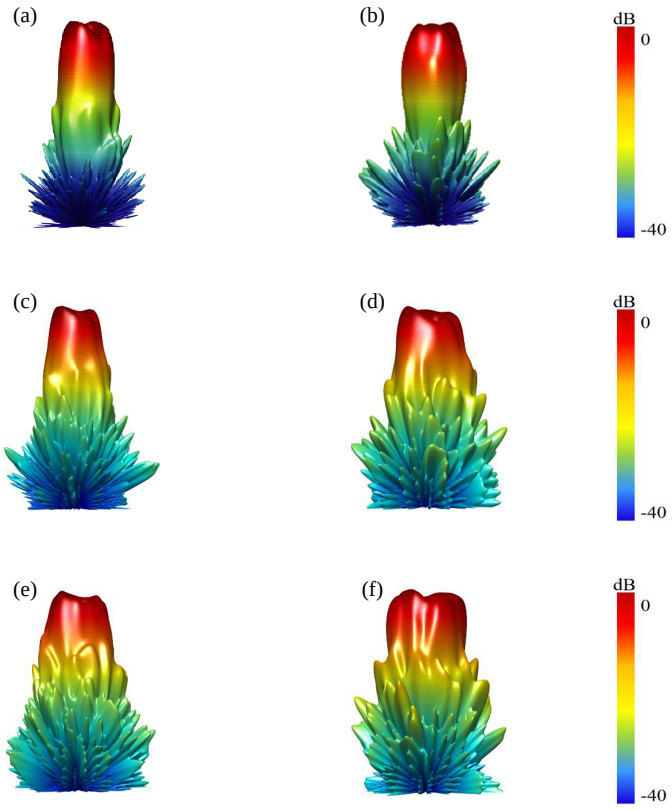

FIGURE 4. The far field of the metasurface and the amplitude and the phase of E-field at 30 GHz: (a), (c), (e) are the OAM of $l = 1, 2, 3$ generated by APMS (controlled by α and β), respectively. (b), (d), (f) are the OAM of $l = 1, 2, 3$ generated by PMS (controlled by β), respectively.

distribution.

$$A_m = A_{\text{final}}/A_{\text{horn}} \tag{16}$$

The final amplitude is shown in Figure 3(b), and Figure 3(c) shows the overall structure diagram. Then, the metasurface units are arranged in an array according to the designed amplitude distribution and the required phase distribution for generating OAM beams. Since the amplitude and phase distributions on the amplitude-phase-controlled surface have been determined, the far-field scattering directivity function can be expressed as:

$$f(\theta,\varphi) = \sum_{m=1}^{M} A(m,n)e^{-j\varphi(m,n)} e^{-jkd\sin\theta[(m-1/2)\cos\phi+(n-1/2)\sin\phi]} \tag{17}$$

where $A(m,n)$ and $\varphi(m,n)$ represent the amplitude and phase of the electromagnetic waves emitted from the (m,n) unit, d is the period of the meta-unit, and θ and φ represent the elevation angle and azimuth angle of the scattering directivity pattern. To compare and analyze the quality of beams generated by phase-only surfaces and amplitude-phase-controlled surfaces, three PMSs and three APMSs with mode numbers of 1, 2, and 3 were simulated using CST with a horn antenna as the excitation source. The cross-polarized far-field scattering directivity patterns obtained from the simulation are shown in Figures 4(a), (c), and (e). It can be seen that compared with OAM beams generated by PMS, the quality of OAM beams generated by APMS is significantly improved. The OAM direction patterns with mode numbers of 1, 2, and 3 have lower sidelobe levels and higher main lobe gain, and the maximum radiation direction is more uniform.

With the determination of amplitude and phase in metasurface, Huygens-Fresnel principle can be used to calculate the radiation field, and the specific formula is as follows [22]:

$$E_{\text{rad}}(r,\theta,\varphi) = C\frac{e^{jkr}}{4\pi r}\iint_{\Omega} E_{af}e^{jk(x\sin\theta\cos\varphi+y\sin\theta\sin\varphi)}\,dxdy \tag{18}$$

where k is the wavenumber, C equal to $jk(1+\cos\theta)$, and E_{af} the aperture field. The calculated amplitude and phase of far field generated by PMS with mode $l = 1$ are as shown in Figures 5(a) and 5(b), respectively. Correspondingly, Figures 5(c) and (d) are far field with the mode $l = 1$ generated by APMS. Comparing APMS with PMS, the calculating results shows that it is effective for CSM to reduce the sidelobes of the generated beams.

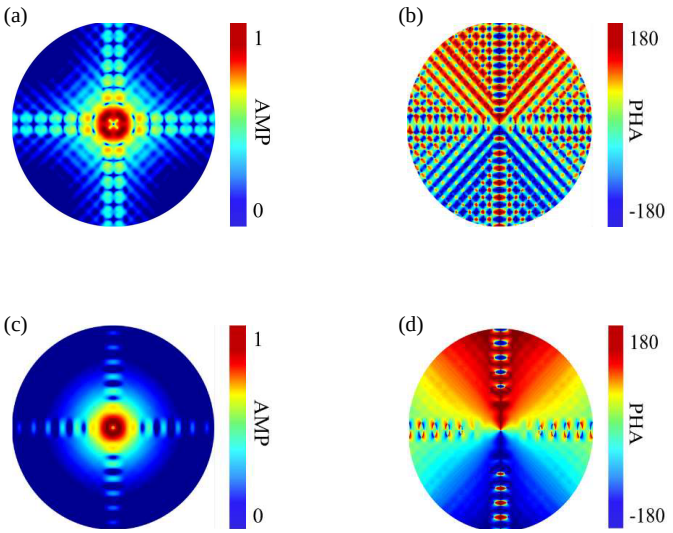

FIGURE 5. Calculated far-field amplitude and phase distribution of the APMS and PMS at 28 GHz with mode $l = 1$: (a) and (b) are the results of PMS, (c) and (d) are the results of APMS.

Based on the complex Fourier transform, we can calculate the OAM mode spectra and mode purity. The first step in analyzing the mode purity is to extract the circular electric field distribution on the cross-section perpendicular to the propagation direction. In this work, the z-coordinate of all sampling planes is 250 mm, which means that all the electric field distribution is needed to extract in sampling plane.

As the azimuthal angle φ is a periodic function, the Fourier transform analysis is implemented on the electric field amplitude and phase distributions in the near-field sampling plane, and the corresponding calculation formula is as follows [21]:

$$A_l = \frac{1}{2\pi}\int_0^{2\pi}\psi(\varphi)e^{-jl\varphi}d\varphi \tag{19}$$

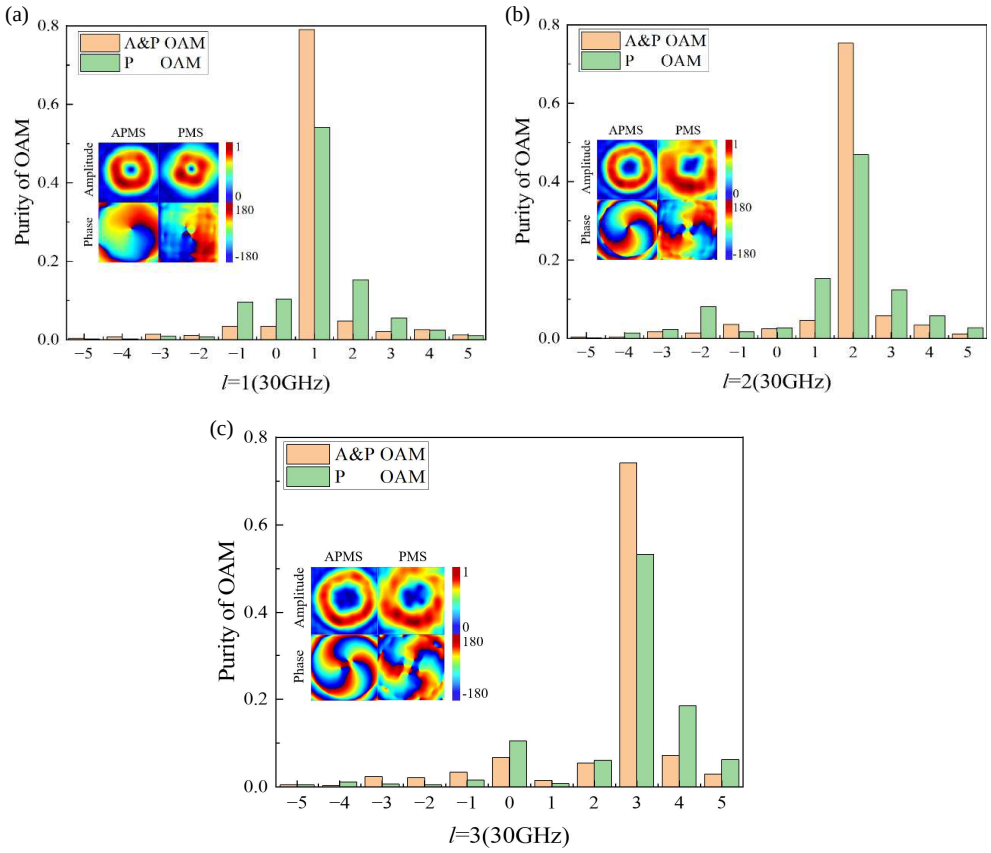

FIGURE 6. The purity of OAM metasurface.

TABLE 1. The comparison of other metasurface.

Reference	Type	Frequency (GHz)	Mode l	Mode purity
[11]	Reflect	18, 28	$-1, 2$	$> 68\%$
[14]	Reflect	5.2, 10.5–12	1, 2	$> 65\%$
[15]	Transmit	28–38	1	$> 72\%$
[21]	Reflect	16–24	$-2, 2$	$> 70\%$
our work	Transmit	22–32	1, 2, 3	$> 75\%$

$$\psi(\varphi) = \sum_{l} A_l e^{jl\varphi} \tag{20}$$

where $\psi(\varphi)$ is the electric field distribution in the sampling plane. To calculate the quality of the generated OAM beams, the mode purity of the OAM beams generated by APMS was analyzed. Due to the characteristics of cross-polarization, the electric field of x-polarization was calculated. Here, the mode spectrum purity from $l = -5$ to $l = 5$ is considered. Defined as a ratio of the dominant mode power over the all modes, the energy weight $P_{\text{energy weight}}$ is defined as:

$$P_{\text{energy weight}} = \frac{A_{l_1}}{\sum_{l=-5}^{5} A_l} \tag{21}$$

The circular electric field distribution of OAM modes with modes $l = 1$, 2, and 3 was Fourier transformed and integrated. Figure 6 shows the corresponding electric field distribution and mode purity of APMS and PMS. The z-coordinate of all sampling planes is 250 mm, and the sampling area is $150 \times 150\,\text{mm}^2$. The purity of vortex beams generated by APMS is 79.02%, 75.35%, and 75.16% with mode $l = 1$, 2, and 3, respectively. Compared with PMS, the purity of three modes increases by 24.96%, 28.49%, and 21.88%, respectively. From Figures 6(a), (b), and (c), it can be seen that the circular amplitude distribution and helical symmetric phase distribution of the OAM beams generated by APMS are more uniform, which further proves the effectiveness of CSM in improving the quality of OAM beams. It can be seen that APMS significantly improves the mode purity of OAM beams because CSM concentrates the energy of the radiation beam in the propagation direction. In addition, the proposed APMS generates OAM modes with smaller mode crosstalk.

Table 1 explain the comparison of the proposed metasurface generating OAM with some published OAM antennas. It can be seen that the proposed metasurface has achieved higher OAM bandwidth with comparable mode purity. It is also pertinent to mention that the proposed metasurface has also achieved

more comprehensive manipulation of electromagnetic waves with OAM mode $l = 1$, 2, and 3.

4. CONCLUSION

In summary, this paper proposes a transmissive APMS. By changing the split angle and direction angle of the split ring, the designed unit can achieve transmission amplitude modulation of 0–1 and transmission phase modulation of 0–360° within a wide frequency band. Therefore, it can be used for precise control of electromagnetic waves. To verify the control performance of the unit, we designed multiple high-quality OAM wave generation surfaces and verified the generation performance of OAM beams on metasurfaces within a wide frequency band. The full-wave simulation and theoretical calculation results are in good agreement, confirming the effectiveness and feasibility of the proposed design method. The proposed APMS extends the range of electromagnetic wave control and is suitable for beam control on metasurfaces.

ACKNOWLEDGEMENT

This work was supported by Chongqing Natural Science Foundation General Program (No. CSTB2022NSCQ-MSX0960).

REFERENCES

[1] Allen, L., M. W. Beijersbergen, R. J. C. Spreeuw, and J. P. Woerdman, "Orbital angular-momentum of light and the transformation of Laguerre-Gaussian laser modes," *Physical Review A*, Vol. 45, No. 11, 8185–8189, Jun. 1992.

[2] Yan, Y., G. Xie, M. P. J. Lavery, H. Huang, N. Ahmed, C. Bao, Y. Ren, Y. Cao, L. Li, Z. Zhao, A. F. Molisch, M. Tur, M. J. Padgett, and A. E. Willner, "High-capacity millimetre-wave communications with orbital angular momentum multiplexing," *Nature Communications*, Vol. 5, 4876, Sep. 2014.

[3] Hui, X., S. Zheng, Y. Hu, C. Xu, X. Jin, H. Chi, and X. Zhang, "Ultralow reflectivity spiral phase plate for generation of millimeter-wave OAM beam," *IEEE Antennas and Wireless Propagation Letters*, Vol. 14, 966–969, 2015.

[4] Cheng, W., W. Zhang, H. Jing, S. Gao, and H. Zhang, "Orbital angular momentum for wireless communications," *IEEE Wireless Communications*, Vol. 26, No. 1, 100–107, Feb. 2019.

[5] Guo, Z.-G. and G.-M. Yang, "Radial uniform circular antenna array for dual-mode OAM communication," *IEEE Antennas and Wireless Propagation Letters*, Vol. 16, 404–407, 2017.

[6] Bai, X., F. Kong, J. Qian, Y. Song, C. He, X. Liang, R. Jin, and W. Zhu, "Polarization-insensitive metasurface lens for efficient generation of convergent OAM beams," *IEEE Antennas and Wireless Propagation Letters*, Vol. 18, No. 12, 2696–2700, Dec. 2019.

[7] Azad, A. K., A. V. Efimov, S. Ghosh, J. Singleton, A. J. Taylor, and H.-T. Chen, "Ultra-thin metasurface microwave flat lens for broadband applications," *Applied Physics Letters*, Vol. 110, No. 22, 224101, May 2017.

[8] Li, H.-P., G.-M. Wang, T. Cai, J.-G. Liang, and X.-J. Gao, "Phase- and amplitude-control metasurfaces for antenna mainlobe and sidelobe manipulations," *IEEE Transactions on Antennas and Propagation*, Vol. 66, No. 10, 5121–5129, Oct. 2018.

[9] Zhang, K., Y. Yuan, X. Ding, H. Li, B. Ratni, Q. Wu, J. Liu, S. N. Burokur, and J. Tan, "Polarization-engineered noninterleaved metasurface for integer and fractional orbital angular momentum multiplexing," *Laser & Photonics Reviews*, Vol. 15, No. 1, 2000351, Jan. 2021.

[10] Ma, Q., C. B. Shi, G. D. Bai, T. Y. Chen, A. Noor, and T. J. Cui, "Beam-editing coding metasurfaces based on polarization bit and orbital-angular-momentum-mode bit," *Advanced Optical Materials*, Vol. 5, No. 23, 1700548, Dec. 2017.

[11] Zhang, L., R. Y. Wu, G. D. Bai, H. T. Wu, Q. Ma, X. Q. Chen, and T. J. Cui, "Transmission-reflection-integrated multifunctional coding metasurface for full-space controls of electromagnetic waves," *Advanced Functional Materials*, Vol. 28, No. 33, 1802205, Aug. 2018.

[12] Xin, M., R. Xie, G. Zhai, J. Gao, D. Zhang, X. Wang, S. An, B. Zheng, H. Zhang, and J. Ding, "Full control of dual-band vortex beams using a high-efficiency single-layer bi-spectral 2-bit coding metasurface," *Optics Express*, Vol. 28, No. 12, 17 374–17 383, Jun. 2020.

[13] Zhang, K., Y. Wang, S. N. Burokur, and Q. Wu, "Generating dual-polarized vortex beam by detour phase: From phase gradient metasurfaces to metagratings," *IEEE Transactions on Microwave Theory and Techniques*, Vol. 70, No. 1, 200–209, Jan. 2022.

[14] Akram, M. R., X. Bai, R. Jin, G. A. E. Vandenbosch, M. Premaratne, and W. Zhu, "Photon spin hall effect-based ultrathin transmissive metasurface for efficient generation of OAM waves," *IEEE Transactions on Antennas and Propagation*, Vol. 67, No. 7, 4650–4658, Jul. 2019.

[15] Ji, C., J. Song, C. Huang, X. Wu, and X. Luo, "Dual-band vortex beam generation with different OAM modes using single-layer metasurface," *Optics Express*, Vol. 27, No. 1, 34–44, Jan. 2019.

[16] Ishfaq, M., X. Li, Z. Qi, W. Zhao, A. Aziz, L. Qiu, and S. Memon, "A transmissive metasurface generating wideband OAM vortex beam in the Ka-band," *IEEE Antennas and Wireless Propagation Letters*, Vol. 22, No. 8, 2007–2011, Aug. 2023.

[17] Bao, L., R. Y. Wu, X. Fu, Q. Ma, G. D. Bai, J. Mu, R. Jiang, and T. J. Cui, "Multi-beam forming and controls by metasurface with phase and amplitude modulations," *IEEE Transactions on Antennas and Propagation*, Vol. 67, No. 10, 6680–6685, Oct. 2019.

[18] Li, H.-P., G.-M. Wang, T. Cai, J.-G. Liang, and X.-J. Gao, "Phase- and amplitude-control metasurfaces for antenna mainlobe and sidelobe manipulations," *IEEE Transactions on Antennas and Propagation*, Vol. 66, No. 10, 5121–5129, Oct. 2018.

[19] Lou, Q. and Z. N. Chen, "Sidelobe suppression of metalens antenna by amplitude and phase controllable metasurfaces," *IEEE Transactions on Antennas and Propagation*, Vol. 69, No. 10, 6977–6981, Oct. 2021.

[20] Rudge, A. W., "Antenna theory and design," *Electronics and Power*, Vol. 28, No. 3, 267, 1982.

[21] Wu, R. Y., L. Bao, L. W. Wu, Z. X. Wang, Q. Ma, J. W. Wu, G. D. Bai, V. Galdi, and T. J. Cui, "Independent control of copolarized amplitude and phase responses via anisotropic metasurfaces," *Advanced Optical Materials*, Vol. 8, No. 11, 1902126, Jun. 2020.

[22] Pan, Y., F. Lan, Y. Zhang, H. Zeng, L. Wang, T. Song, G. He, and Z. Yang, "Dual-band multifunctional coding metasurface with a mingled anisotropic aperture for polarized manipulation in full space," *Photonics Research*, Vol. 10, No. 2, 416–425, Feb. 2022.

[23] Jiang, S., C. Chen, J. Ding, H. Zhang, and W. Chen, "Alleviating orbital-angular-momentum-mode dispersion using a reflective metasurface," *Physical Review Applied*, Vol. 13, No. 5, 054037, May 2020.